Sādhanā Vol. 39, Part 3, June 2014, pp. 713–729. © Indian Academy of Sciences

Turbulent jet in confined counterflow

M SIVAPRAGASAM[1]*, M D DESHPANDE[1], S RAMAMURTHY[2] and P WHITE[3]

[1]Department of Automotive and Aeronautical Engineering, M S Ramaiah School of Advanced Studies, Bangalore 560 058, India
[2]National Civil Aircraft Development Programme, National Aerospace Laboratories, Bangalore 560 017, India
[3]Faculty of Engineering and Computing, Coventry University, Coventry CV1 5FB, UK
e-mail: msp@msrsas.org

MS received 26 November 2012; revised 9 November 2013; accepted 21 November 2013;

Abstract. The mean flowfield of a turbulent jet issuing into a confined, uniform counterflow was investigated computationally. Based on dimensional analysis, the jet penetration length was shown to scale with jet-to-counterflow momentum flux ratio. This scaling and the computational results reproduce the well-known correct limit of linear growth of the jet penetration length for the unconfined case when the momentum flux ratio is small. However, for the high momentum flux ratio case corresponding to the confinement, the jet penetration length is shown to reach an asymptotic limit of about 3.57 times the confining duct diameter. This conclusion is contrary to the existing results which predict indefinite growth. A simple modification of an existing similarity solution for the jet in an unconfined counterflow provides a convenient framework for presenting the results of the flowfield and jet penetration length.

Keywords. Turbulent jet; counterflow; penetration length; computational fluid dynamics; similarity solution.

1. Introduction

A turbulent jet is a basic free shear flow and has received research attention (see, for example, Pope 2000). However, in many engineering applications the jet does not issue into a quiescent stream but interacts with an external stream. This interaction can be classified as co-flow, crossflow or counterflow depending on the direction of interaction between the jet and the external stream. Of these interactions, the jet in counterflow is the least investigated because of the extreme theoretical and experimental difficulties associated with the reverse flow phenomenon and marked instability of the flow. Interestingly, these flow characteristics which are responsible

*For correspondence

for the complexity of the flow also lead to enhanced mixing thus rendering the jet in counterflow configuration suitable for various mixing and combustion applications.

Of the relatively few studies available on the turbulent jet in counterflow, most of them consider the flowfield to be *unconfined*. Under this realisation, the jet penetration length is linearly proportional to the velocity ratio between the jet and the counterflow (Arendt *et al* 1956; Beltaos & Rajaratnam 1973; Yoda & Fiedler 1996; Lam & Chan 1997; Chan & Lam 1998; Bernero 2000). The turbulent jet in *confined* counterflow was studied by Sekundov (1969), Morgan *et al* (1976), Saghravani & Ramamurthy (2010). The effect of confinement is a reduction in the penetration length and more importantly departure from the linear jet penetration length-velocity ratio relation.

The present study pertains to the computational evaluation of the penetration length of a turbulent jet issuing into a confined, uniform counterflow. A series of computations was performed for different jet-to-counterflow velocity ratios and for various duct-to-jet diameter ratios extending the range of parameters. The results compared well with the experimental data of Morgan *et al* (1976) (MBE76 hereafter). The results of Oron & Abuaf (1977) (OA77 hereafter) for an unconfined counterflow using a similarity solution provide a theoretical framework for presenting the present results. However, the developing region of the jet with the potential core does not form a part of this similarity region. After adding the length of the developing region, a good agreement with the similarity results of OA77 was seen. It is instructive to see the effects of confinement also in the same plot. By extending the range of the two parameters involved we are able to make interesting observations.

The present paper is arranged as follows. The description of the flowfield under consideration is described in section 2 followed by details of the computational procedure in section 3. The jet penetration length obtained from the computations is compared with available experimental results in section 4. The momentum flux scaling relation of MBE76 is used extensively to present the jet penetration length. The similarity solution of OA77 is presented in section 5 accompanied by a critical discussion in the light of our computational results. The regions of validity of the similarity solution are highlighted. The decay of jet centreline velocity is presented and it is found that similarity is found at least for high velocity ratio jets at large values of diameter ratio. The effect of jet exit turbulence intensity is also investigated and reported in section 6, and conclusions are provided in section 7.

2. Description of the flowfield

Consider a steady, incompressible, turbulent jet of velocity u_j issuing from a nozzle of diameter d_j into a steady uniform stream of velocity u_0 ($u_j > |u_0|$) confined within a duct of diameter D_0 as shown in figure 1. The direction of freestream velocity is opposite to that of the jet. The ratio of jet-to-counterflow velocity is u_j/u_0 and the ratio of the diameters of the confining duct and the jet nozzle is D_0/d_j.

The jet penetrates into the counterflow stream up to a certain distance, then interacts with the freestream and deflects backwards. This length, measured on the jet axis, from the nozzle exit till where the axial velocity becomes zero is termed the penetration length, l_p.

The axial extent of the jet can be divided into three distinct regions (Sekundov 1969). The region immediately downstream of the jet nozzle consists of a developing jet with the potential core of the jet and persists downstream for a few nozzle diameters. In the potential core the velocity is uniform and equal to u_j. The jet beyond the developing region, in region 2, qualitatively behaves like a free jet. Later, in this paper, it will be seen that a similarity solution exists

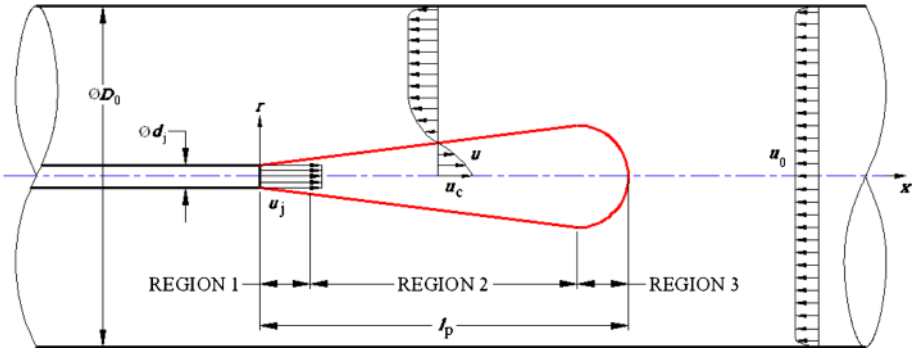

Figure 1. Schematic description of the flowfield. The jet-to-counterflow velocity ratio is u_j/u_0; the diameter ratio is D_0/d_j.

in this region. The jet thickness increases with distance from the nozzle. The jet and the counterflow stream interact intensely in region 3 and this region is characterized by a highly turbulent field of flow.

3. Computational procedure

The governing equations of mass and momentum conservation for a turbulent flowfield namely, the Reynolds-averaged Navier–Stokes equations, are solved numerically using the commercial software ANSYS FLUENT. The time-averaged computations were performed for a range of diameter ratios, D_0/d_j, from 3 to 100 and jet-to-counterflow velocity ratios, u_j/u_0, ranging from 2 to 250. The counterflow stream inlet was placed at a distance 100 d_j for $D_0/d_j = 3$ to 30 and at 700 d_j for $D_0/d_j = 100$, respectively ahead of the jet exit. The flow domain outlet was at 100 d_j behind the jet exit.

An axisymmetric structured grid was devised for the computations. The computational domain for the numerical solution consisted of 1000 axial $\times$ 25 radial (axis to wall) non-uniform cells for $D_0/d_j = 3$; 1000 $\times$ 45 for $D_0/d_j = 5$; 1000 $\times$ 95 for $D_0/d_j = 10$; 1000 $\times$ 145 for $D_0/d_j = 15$; 1000 $\times$ 325 for $D_0/d_j = 30$; and 5200 $\times$ 510 for $D_0/d_j = 100$ (i. e., 2,652,000 cells). The number of computational cells was chosen after a careful grid independence study. This study was conducted for the D_0/d_j = 10, $u_j/u_0 = 20$ case with 52,000 (coarse grid), 95,000 (medium grid) and also with 150,000 (fine grid) grid points. The Grid Convergence Index (see Celik *et al* 2008) was calculated and the numerical uncertainty in the calculation of jet penetration length in terms of the discretisation error is 0.99% and 1.45% for the fine and medium grids, respectively. The apparent order of the numerical method was calculated to be about 1.65. Since the medium grid had a reasonably low value of discretisation error it was employed and grids for the other cases were constructed with similar grid spacing, particularly in the jet penetration region, thus ensuring an acceptably low discretisation error.

The computations were performed using the standard k-ε turbulence closure model. All calculations were carried out in double-precision arithmetic. The Reynolds number (Re) of the counterflow stream (based on D_0 and u_0) varied from 10^4 to 3 $\times 10^5$ and that of the jet (based on d_j and u_j) varied from 6 $\times 10^3$ to 6 $\times 10^4$. The values of Reynolds number used in the present computations meet the requirements stipulated by MBE76 for results being independent of Reynolds number. Some select calculations also showed that the present results were independent of the Reynolds number.

4. Results

4.1 *Velocity field*

The mean streamlines in the flowfield are shown in figure 2, for a diameter ratio of 10 and a velocity ratio of 20. The jet originating from the nozzle and penetrating into the counterflow stream can be clearly seen. The flowfield is dominated by a large recirculation region as observed in this figure. The flowfield can be reckoned into three parts different from those shown in figure 1. There is a toroidal shaped eddy in the jet region. The flow from the jet penetrates this eddy, wraps around and returns backwards. The counterflow stream is distinct from the jet flow, the two streams being separated by a dividing stream surface. The counterflow stream does not come into contact with this eddy. The profiles of axial velocity in the radial direction at various locations are shown in the bottom half of figure 2.

4.2 *Jet penetration length*

The jet penetration length, l_p, is defined as the length of the jet from the nozzle exit to a point on the axis where the axial velocity becomes zero. The penetration length depends on the jet-to-counterflow velocity ratio, u_j/u_0, and on the duct-to-jet diameter ratio, D_0/d_j. Thus, in the non-dimensional form

$$\frac{l_p}{d_j} = f\left(\frac{u_j}{u_0}, \frac{d_j}{D_0}\right) \quad . \tag{1}$$

For an unconfined counterflow case this relation reduces to

$$\frac{l_p}{d_j} = f\left(\frac{u_j}{u_0}\right) \quad . \tag{2}$$

It is possible to evaluate this functional form from dimensional analysis itself by taking jet momentum as a parameter. This leads to a linear relation (see also Arendt *et al* 1956; Beltaos & Rajaratnam 1973)

$$\frac{l_p}{d_j} = c\frac{u_j}{u_0}. \tag{3}$$

The value of the linearity constant c is quoted by various investigators to be in the range from 2.4 to 2.9. Several factors might have influenced this variation in c. To list a few, we may mention, (i) different boundary conditions at the jet exit and the counterflow stream inlet,

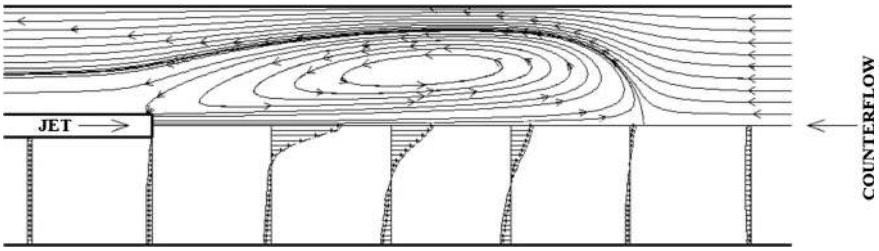

Figure 2. Mean streamlines in the flowfield are shown in the top half of this figure. The profiles of axial velocity in the radial direction at various locations are shown in the bottom half; $D_0/d_j = 10$ and $u_j/u_0 = 20$.

(ii) different values of turbulence intensity in the two streams and (iii) influence of the confining duct for larger values of u_j/u_0. It may be noted, however, that the variation in c is not substantial.

The penetration length l_p/d_j evaluated from the present computation was compared with the experimental data of MBE76 and a reasonably good agreement was observed. This length from the present computations is shown in figure 3.

A remarkable collapse of the penetration length data was achieved in MBE76 by plotting l_p/D_0 as a function of jet-to-counterflow momentum flux ratio. This ratio is

$$Z = \left(\frac{u_j d_j}{u_0 D_0}\right)^2, \tag{4}$$

since density, ρ, is constant. From their experimental results they divided the flow into two distinct regimes based on the momentum flux ratio (see figure 4a). When the counterflow momentum flux is high compared to the jet momentum flux ($\sqrt{Z} < 0.5$) the penetration length is linearly related to the velocity ratio. This relationship is of the form

$$\frac{l_p}{D_0} = 2.9\left(\frac{u_j d_j}{u_0 D_0}\right), \tag{5}$$

which reduces back to the earlier form (Eq. 3)

$$\frac{l_p}{d_j} = 2.9\frac{u_j}{u_0}. \tag{6}$$

The linearity constant, c, is chosen here to be 2.9 as against 2.5 suggested in MBE76.

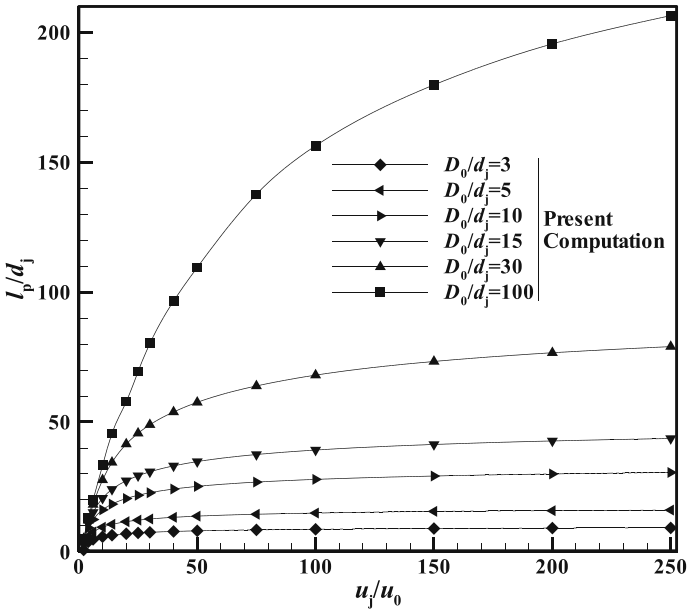

Figure 3. Non-dimensional jet penetration length, l_p/d_j, plotted as function of jet-to-counterflow velocity ratio, u_j/u_0.

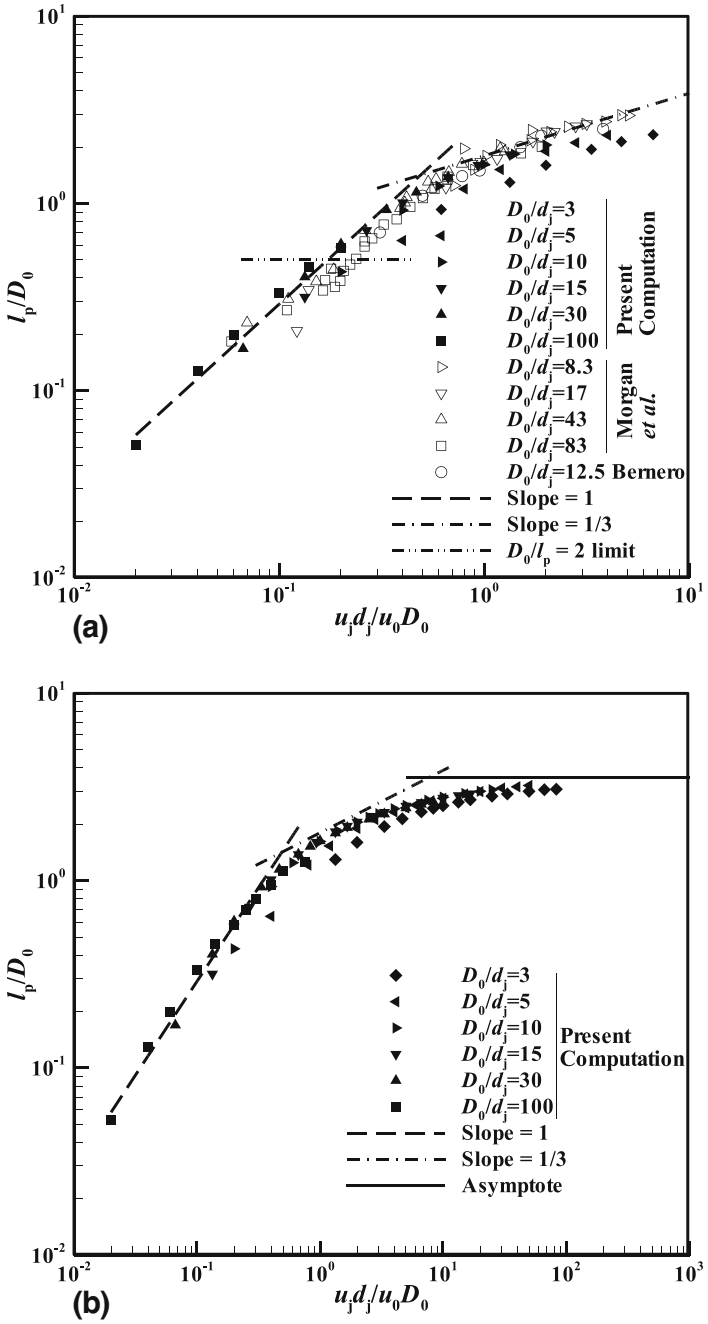

Figure 4. Non-dimensional jet penetration length, l_p/D_0, as a function of the jet-to-counterflow momentum flux ratio parameter, $u_j d_j/u_0 D_0$. **(a)** Initial computational results compared with the experimental data of Morgan *et al* (1976), and Bernero (2000); the linear and one-third power law are shown here. The limit for unconfined jet $D_0/l_p \geq 2$ (Sekundov 1969) is also indicated. **(b)** Extended computational results with the linear and one-third power law. The asymptotic limit for the jet penetration length of about 3.57 D_0 is also depicted.

As the value of Z increases further, the influence of confinement becomes effective for a range of

$$0.5 < \sqrt{Z} < 1.5. \tag{7}$$

MBE76 identify this to be a transitional zone and for $\sqrt{Z} > 1.5$ suggest a one-third power law, and then the penetration length is given by

$$\frac{l_\mathrm{p}}{D_0} = 1.8 \left(\frac{u_j d_\mathrm{j}}{u_0 D_0} \right)^{\frac{1}{3}}. \tag{8}$$

The authors did not provide any explanation as to why data should collapse so neatly with the modified coordinates and also to such a simple relation for the confined case with $\sqrt{Z} > 1.5$. The two regimes of MBE76 were also reiterated by one of these authors elsewhere (Brinkworth 1999). In the present study, a dimensional analysis is carried out first using jet momentum flux, counterflow stream velocity u_0 and the diameters D_0 and d_j which led us to the relation

$$\frac{l_\mathrm{p}}{D_0} = f \left(\frac{u_j d_\mathrm{j}}{u_0 D_0} \right). \tag{9}$$

This explains the data collapse as first indicated in MBE76. However, the present observations differ qualitatively from those in MBE76.

Also shown in figure 4a is the criterion for the jet expanding in counterflow of infinite extent. Sekundov (1969) indicated that the flowfield may be considered to be unconfined if $D_0/l_\mathrm{p} \geq 2$. This limit is shown in figure 4a and the data points below this line are for unconfined flow.

As the effect of confinement increases, the penetration length seems to follow the one-third power law beyond a transitional zone. However, a closer examination of the results in figure 4a in the high jet momentum regime reveals that the agreement with the one-third power law is not satisfactory, particularly in the presence of significant confinement where the power appears to drop gradually to less than 1/3. This raised an important question as to whether, if at all, a power-law behaviour would govern the jet penetration length at high momentum ratios. This led us to investigate the jet penetration length behaviour at very high momentum ratios; the velocity ratio was increased up to 250 which corresponded to a momentum flux ratio of about 7,000 for a diameter ratio of three.

The extended computational results are plotted in figure 4b. It is now clear that the one-third power law is not valid for high momentum flux ratios. More importantly, there is no distinct regime 2 unlike a clearly identified regime 1. The experiments of MBE76 had covered a momentum flux ratio up to about 25 and within this range they inferred the one-third power law approximating their experimental data. However, as is evident from the present investigation the slope of this curve continuously decreases and asymptotically tends to zero. The asymptotic value for the maximum jet penetration length is estimated to be 3.57 times the diameter of the enclosing duct. This value was obtained by averaging the asymptotic limits for each of the D_0/d_j cases which were themselves estimated by extrapolating the present computational results.

The fact that the jet penetration length does not increase indefinitely can be seen readily from figure 3 where the jet length is plotted as a function of the velocity ratio. The curves for each of the diameter ratios considered do, indeed, tend to a constant value after a finite velocity ratio.

The existence of an asymptotic limit for the jet penetration length can also be explained referring to the mean streamline pattern in figure 2. There is a toroidal shaped eddy in the jet region. The flow from the jet penetrates this eddy, wraps around and returns backwards. The counterflow stream is distinct from the jet flow, the two streams being separated by a dividing stream

surface. The counterflow stream does not come in contact with this eddy. As the jet momentum flux increases the eddy length increases and the dividing stream surface is pushed forward. This forward force is proportional to the jet momentum and is independent of the penetration length l_p. The force on the dividing stream surface in the negative direction scales like $(u_0^2 d_e^2)$ as long as the eddy diameter d_e is small compared to D_0. Since d_e grows with l_p the rate of growth of both these scales should slow down once d_e becomes comparable to D_0. Then the reverse jet flow and the counterflow stream have to pass through a narrower and longer annular region. The additional force in the negative direction scales like $(u_0 D_0^2 l_p / g^2)$, where g is the narrow gap $(D_0 - d_e)/2$. Because of this sharp increase, eventually it is not possible for the jet to push the eddy forward no matter how high the momentum. There is no such restriction in the unconfined case.

The counterflow stream passes through an annular converging–diverging geometry formed by the dividing stream surface. The pressure drop in the counterflow mainly occurs in the converging part but the minimum pressure value occurs slightly towards the downstream side of the throat (left side of the throat in figure 2). The maximum velocity in this neighbourhood u_{max} non-dimensionalised by u_0 grows *linearly* in u_j/u_0 for all diameter ratios D_0/d_j as shown in figure 5. This interesting observation can be explained from the fact that a higher u_j results in a higher return flow and also higher velocity from counterflow due to a narrower gap thus leading to higher u_{max}/u_0 and hence the indefinite growth.

The observation of MBE76 that high momentum jets are sternly restrained by the counterflow stream and the confining duct is correct. The present results strengthen it further by qualifying that the restraining is to a finite penetration length no matter how high the jet momentum flux.

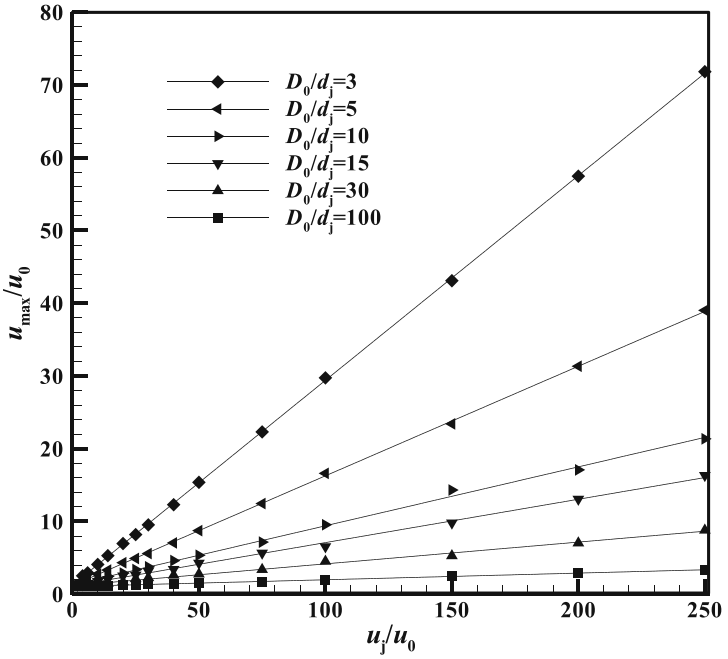

Figure 5. Maximum counterflow velocity in the neighbourhood of the jet, u_{max}, non-dimensionalised by the counterflow stream velocity u_0, is plotted for different u_j/u_0. It can be seen that this ratio grows linearly and indefinitely.

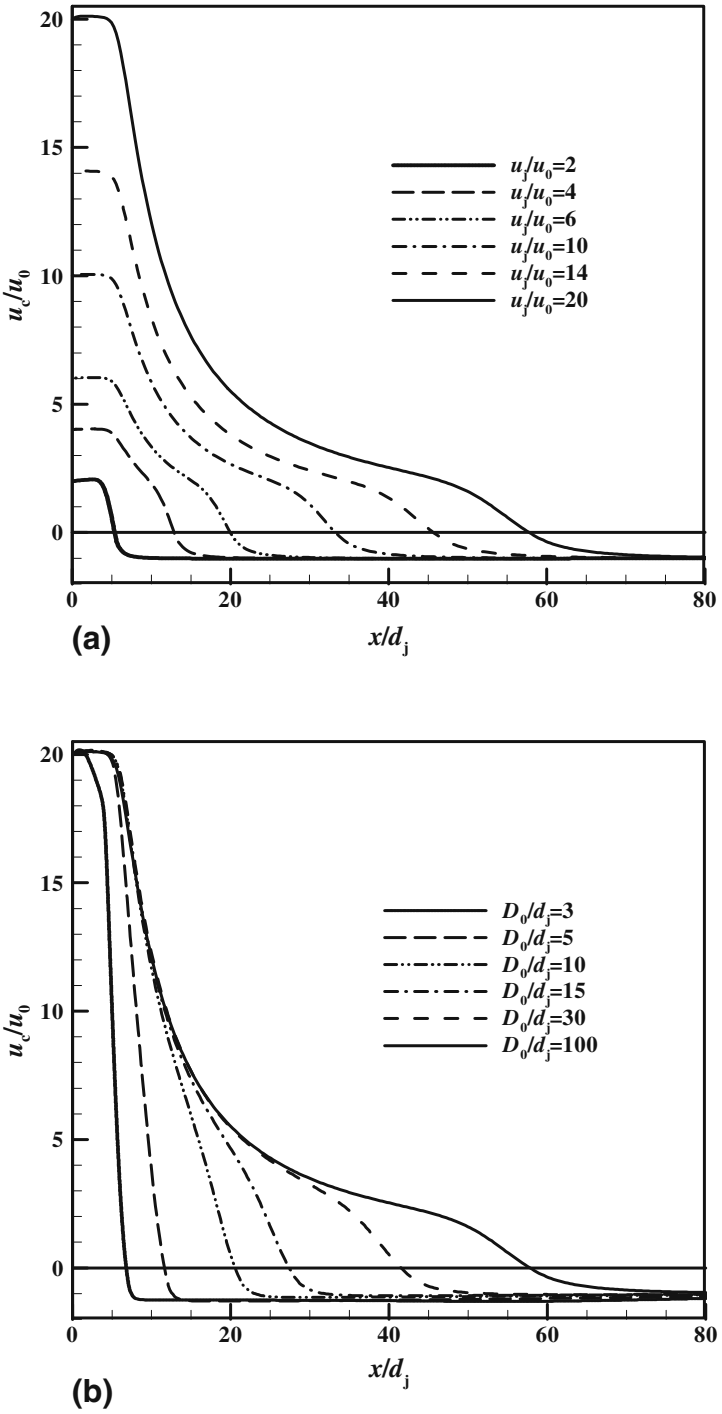

Figure 6. Variation of axial velocity along jet centreline, u_c/u_0. **(a)** $D_0/d_j = 100$ **(b)** $u_j/u_0 = 20$. The similarity region starts beyond the developing region and persists till the jet interacts with the counterflow stream intensely as indicated by a sudden change in the slope.

Another question needs to be addressed here. Why is it that the result of dimensional analysis as given by Eq. (9) shows larger scatter in figure 4b for intermediate values of momentum flux ratios? The primary reason for this is the length of the potential core which is part of the jet penetration length. The potential core length is fairly constant and unaffected by the counterflow and its length is a substantial part of the penetration length. It is equivalent to other parameters being introduced in the dimensional analysis of the problem leading to the scatter. We will discuss these issues in the next section.

4.3 *Variation of centreline velocity*

The decay of axial velocity along the jet centreline, u_c, for a diameter ratio of 100 at different velocity ratios is plotted in figure 6a. The jet issuing out of the nozzle forms a developing region with a central potential core. This was identified as region 1 in figure 1. The similarity region commences beyond the developing region (region 2 in figure 1). The jet intensely interacts with the counterflow stream in region 3. This interaction causes the jet to deflect backwards as can be seen from the streamline plots in figure 2. A drastic change in the centreline velocity slope identifies end of the similarity region 2 and a stronger interaction between the two streams begins. It may also be noticed that at the lowest velocity ratio of two, the jet penetration length is too small, and the counterflow starts interacting with the jet right at the end of the potential core.

The effect of confinement on the centreline velocity can be seen from figure 6b where it is plotted for a velocity ratio of 20 for different confinement ratios. The length of the developing region is hardly affected by the confinement and in the similarity region the velocity profile u_c/u_0 does not depend on the diameter ratio. However, the length of the similarity region is shortened due to more severe confinement. Also, the length of the interaction region is not very sensitive to the diameter ratio.

5. Similarity solution of Oron & Abuaf (1977)

A similarity solution (Oron & Abuaf 1977) exists for the flowfield in region 2 (see figure 1) for the unconfined case, i.e., D_0/d_j being very large. We start with this solution so that a rational basis can be obtained for predicting the penetration length. This will lead us to a logical framework for comparing the jet penetration length with the computational results even in the presence of confinement.

The similarity solution for a turbulent jet in an unconfined counterflow obtained by OA77 is briefly described in this section. The governing equations for the axisymmetric flowfield are written below following the usual boundary layer assumptions:

$$\left(u\frac{\partial u}{\partial x}+v\frac{\partial u}{\partial r}\right)=\frac{1}{\rho}\frac{1}{r}\frac{\partial}{\partial r}\left(r\mu_t\frac{\partial u}{\partial r}\right) \tag{10}$$

$$\frac{\partial}{\partial x}(ru)+\frac{\partial}{\partial r}(rv)=0, \tag{11}$$

subject to the boundary conditions

$$v=0,\ \frac{\partial u}{\partial r}=0 \text{ at } r=0, \text{ and} \tag{12}$$

$$u=-u_0 \text{ as } r\to\infty. \tag{13}$$

At the jet exit ($x = 0$),

$$m_{\mathrm{j}} = \rho \int_0^{r_{\mathrm{j}}} 2\pi u\,(0, r)\, r\, dr, \quad \text{and} \tag{14a}$$

$$u\left(0, r_{\mathrm{j}}\right) = 0. \tag{14b}$$

Here, ρ is the density of the fluid, m_{j} is the jet mass flow rate and $r_{\mathrm{j}} = d_{\mathrm{j}}/2$, is the radius of the jet nozzle (see figure 1). The turbulent viscosity, μ_{t}, is modelled using a modified version of the Prandtl mixing length model for free shear flows (see Schlichting 1979).

A similarity solution is attempted assuming that the streamfunction ψ is of the form

$$\psi = U \Delta f\,(\eta)\,. \tag{15}$$

Here, Δ is a characteristic cross-sectional mixing area in the radial direction, $\eta = \Gamma/\Delta$, and U is the relative velocity defined as $U = u_{\mathrm{c}} + u_0$; u_{c} is the axial velocity along the x-axis and is a function of x only.

Also, Γ is a new variable defined as $\Gamma = \int_0^r r\, dr = \frac{r^2}{2}$.

Substituting the assumed form of the similarity solution (15) in Eqs. (10) and (11), the following expression was obtained for the variation of axial velocity along the jet centreline:

$$\frac{l_{\mathrm{p}} - x}{d_{\mathrm{j}}} = \frac{1}{2\lambda} \frac{e^{\eta_{\mathrm{j}} - 1}}{\sqrt{2\eta_{\mathrm{j}}}} \left[1 - \frac{u_0}{U} \exp\left(1 - \frac{u_0}{U}\right)\right], \tag{16}$$

where η_{j} is the value of η at the starting location of the jet similarity and $\lambda = 0.075$ is the non-dimensional value of mixing length in the jet.

If at $x = 0$, the relative velocity $U = U_0$, the jet penetration length, lp, can be obtained from:

$$\frac{l_{\mathrm{p}}}{d_{\mathrm{j}}} = \frac{1}{2\lambda} \frac{e^{\eta_{\mathrm{j}} - 1}}{\sqrt{2\eta_{\mathrm{j}}}} \left[1 - \exp\left(1 - \eta_{\mathrm{j}} - e^{-\eta_{\mathrm{j}}}\right)\right]. \tag{17}$$

5.1 *Application of similarity solution to nozzles with uniform velocity profiles*

It is to be noted that in the derivation of the expressions (16) and (17) above, OA77 assumed a fully developed velocity profile at the nozzle exit. They also extended their analysis to nozzles with a uniform velocity profile at the jet exit. The velocity ratio, u_{j}/u_0, was related to η_{j} through an approximation

$$\eta_{\mathrm{j}} = \ln\left(1 + \frac{u_{\mathrm{j}}}{u_0}\right). \tag{18}$$

A hypothetical nozzle was defined at the end of the developing region which can be used to evaluate the penetration length beyond this location from Eq. (17). Hence in Eqs. (16) and (17) d_{j} is actually the diameter of the hypothetical nozzle d_{h}, which needs to be replaced by the physical diameter d_{j}. This was done in OA77 by approximating

$$\frac{d_{\mathrm{h}}}{d_{\mathrm{j}}} = \sqrt{2\eta_{\mathrm{j}}}. \tag{19}$$

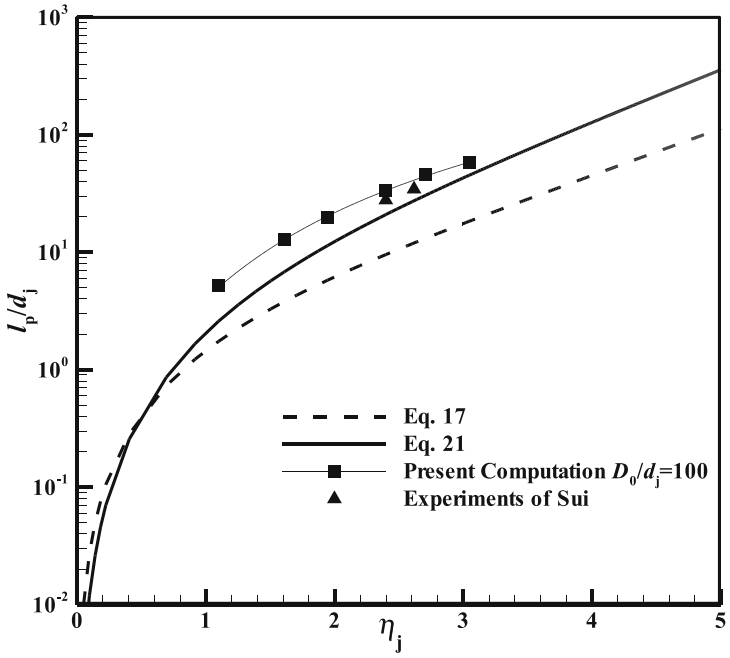

Figure 7. Non-dimensional jet penetration, l_p/d_j, as a function of η_j from Oron & Abuaf (1977). The dashed line is Eq. (17) and the dark continuous curve is Eq. (21) accounting for the hypothetical nozzle diameter given by Eq. (19).

Thus, Eqs. (16) and (17) get modified, respectively, to

$$\frac{l_p - x}{d_j} = \frac{1}{2\lambda} e^{\eta_j - 1} \left[1 - \frac{u_0}{U} \exp\left(1 - \frac{u_0}{U}\right)\right], \tag{20}$$

and

$$\frac{l_p}{d_j} = \frac{1}{2\lambda} e^{\eta_j - 1} \left[1 - \exp\left(1 - \eta_j - e^{-\eta_j}\right)\right]. \tag{21}$$

The jet penetration lengths calculated from the OA77 model using Eqs. (17) and (21) using the actual and hypothetical nozzle diameters are plotted in figure 7 and compared with the present computational results for the highest diameter ratio $D_0/d_j = 100$ in the study. It can be seen that the OA77 model highly under-predicts the jet penetration length.

A major difficulty in this comparison is not knowing where exactly the hypothetical nozzle is to be located and hence the approximation given by Eq. (19) is inadequate. Also, the penetration length starts from this hypothetical nozzle and such data will neither be available nor convenient to a designer or an experimenter. Even though OA77 claim a good agreement with modified experimental data of Sui (taken from Sekundov 1969), they had to curtail a significant portion of the jet length (more than 50% in some cases).

To overcome this difficulty we account for the distinct potential core of length l_c (see Eq. 22) and also modify the approximations given by Eqs. (20) and (21) by introducing a scaling factor α to write

$$\frac{l_p - x}{d_j} = \frac{\alpha}{2\lambda} e^{\eta_j - 1} \left[1 - \frac{u_0}{U} \exp\left(1 - \frac{u_0}{U}\right)\right]. \tag{22}$$

Further, the procedure is simplified in this model assuming that similarity starts from the distinct location where the potential core ends; the determination of the length of the potential core is straightforward. This enables us to add the length of the potential core to the length of the similarity region to obtain the jet penetration length.

Now the computational data are useful in the evaluation of the scaling factor α. This is shown in figure 8. Again, the case of $D_0/d_j = 100$, the highest diameter ratio computed is considered. There is a reasonably good agreement after a shift equivalent to the potential core length is made. The advantage here compared to the strategy of OA77 is that this location is distinct and easily identified and this length is not very sensitive to the velocity ratio u_j/u_0, at least for large values of velocity ratios which are of practical interest.

Another superior feature of the procedure is that the overall jet penetration length is kept intact unlike in OA77 where the comparison is made with a curtailed penetration length. The value of α used here is 1.3 for all cases of u_j/u_0.

A particularly important observation to be made in figure 8 is when the centreline velocity, u_c/u_0, becomes negative after the curve reaches the stagnation point. This is given by a dotted curve and it does not represent the physical reality. The results given by Eqs. (16), (20), or (22) do not have validity beyond the penetration length. The tangent to this curve at the stagnation point is, in fact, vertical and this shows the difficulty in achieving good agreement between the actual and similarity solutions in this neighbourhood. This difficulty, of course, is not unexpected since the boundary layer assumptions themselves fail in the neighbourhood of the stagnation point.

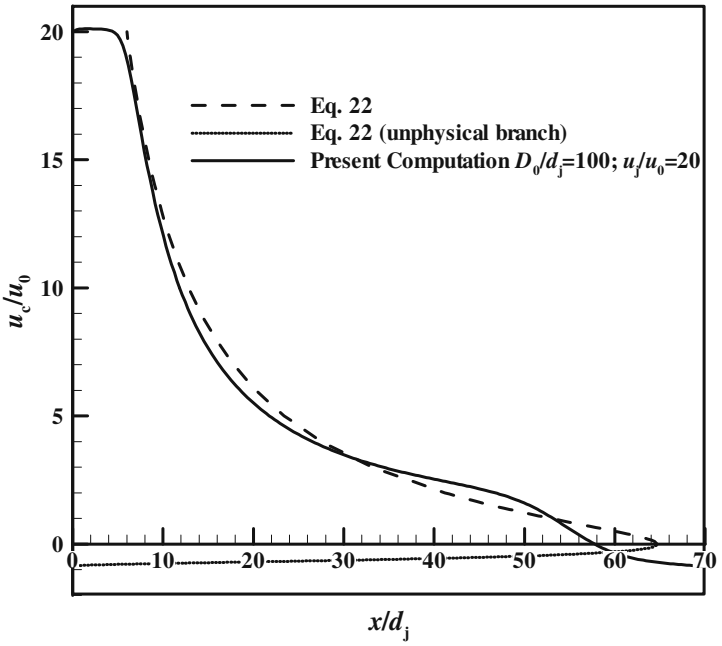

Figure 8. Variation of axial velocity, u_c/u_0, along the jet centreline; $u_j/u_0 = 20$. The variation of jet centreline velocity given by Oron & Abuaf (1977) modified by a scaling factor as given in Eq. (22) is plotted here. This equation does not give values beyond the stagnation point and gives negative centreline velocity which is not physical and is shown by a dotted curve.

A further insight into the similarity solution and the flow may be obtained by replotting figure 8 on a logarithmic scale as shown in figure 9 in order to examine if any power law exists for the decay of centreline velocity. The ordinate now chosen is the centreline axial velocity, u_c, non-dimensionalised by the relative velocity U ($U = u_c + u_0$). By plotting the reciprocal of u_c we see a convincing power law with slope = 1 and agreement between the computational and similarity solutions after the similarity solution is shifted to the right by the length of the potential core. The boundaries of the three regions shown schematically in figure 1 can clearly be seen here. The similarity solution has difficulty in the vicinity of the stagnation point as explained above. The equivalent of the dotted line in figure 8 is ignored here. Further, it may be mentioned that the centreline velocity in a free round jet is like x^{-1} with a shifted virtual origin. Hence it is not surprising that we see slope = 1 in this figure.

A comment on the length of the interaction region (region 3 in figure 1) is appropriate here. OA77 estimate this region to extend from $u_c/u_0 = 0.22$ till the stagnation point. The present results are contrary to this observation. The interaction region starts earlier where u_c/u_0 falls below 2 (see figure 6a). As mentioned above, this observation will not affect the overall results as this length constitutes only a small part of the jet penetration length.

Thus the modelled jet penetration length can finally be written as,

$$\frac{l_p}{d_j} = \frac{\alpha}{2\lambda} e^{\eta_j - 1}\left[1 - \exp\left(1 - \eta_j - e^{-\eta_j}\right)\right] + \frac{l_c}{d_j}. \tag{23}$$

Here, l_c is the potential core length whose values were evaluated from the present computational results. As mentioned earlier this length is not very sensitive to the velocity ratio, u_j/u_0.

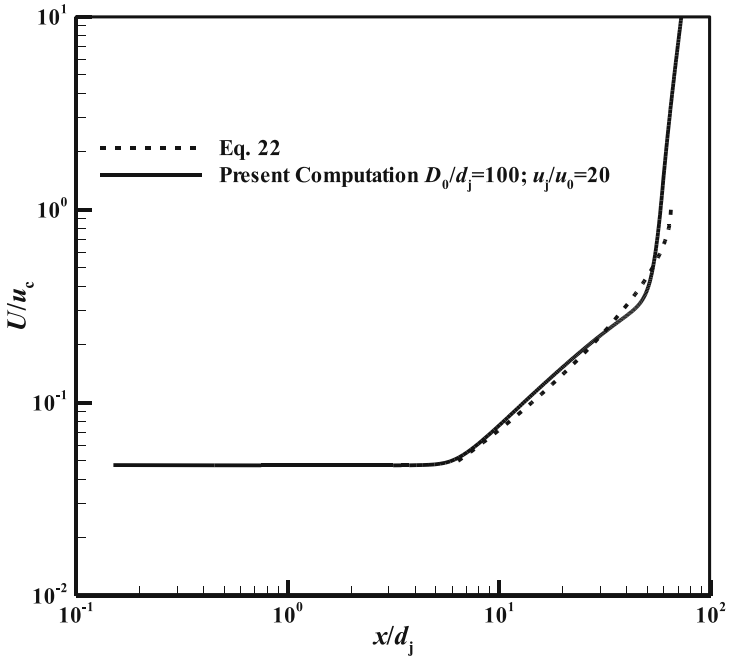

Figure 9. Variation of axial velocity along jet centreline plotted as a function of the axial location. Plotting the reciprocal of u_c helps to identify a power law-like variation in the similarity region.

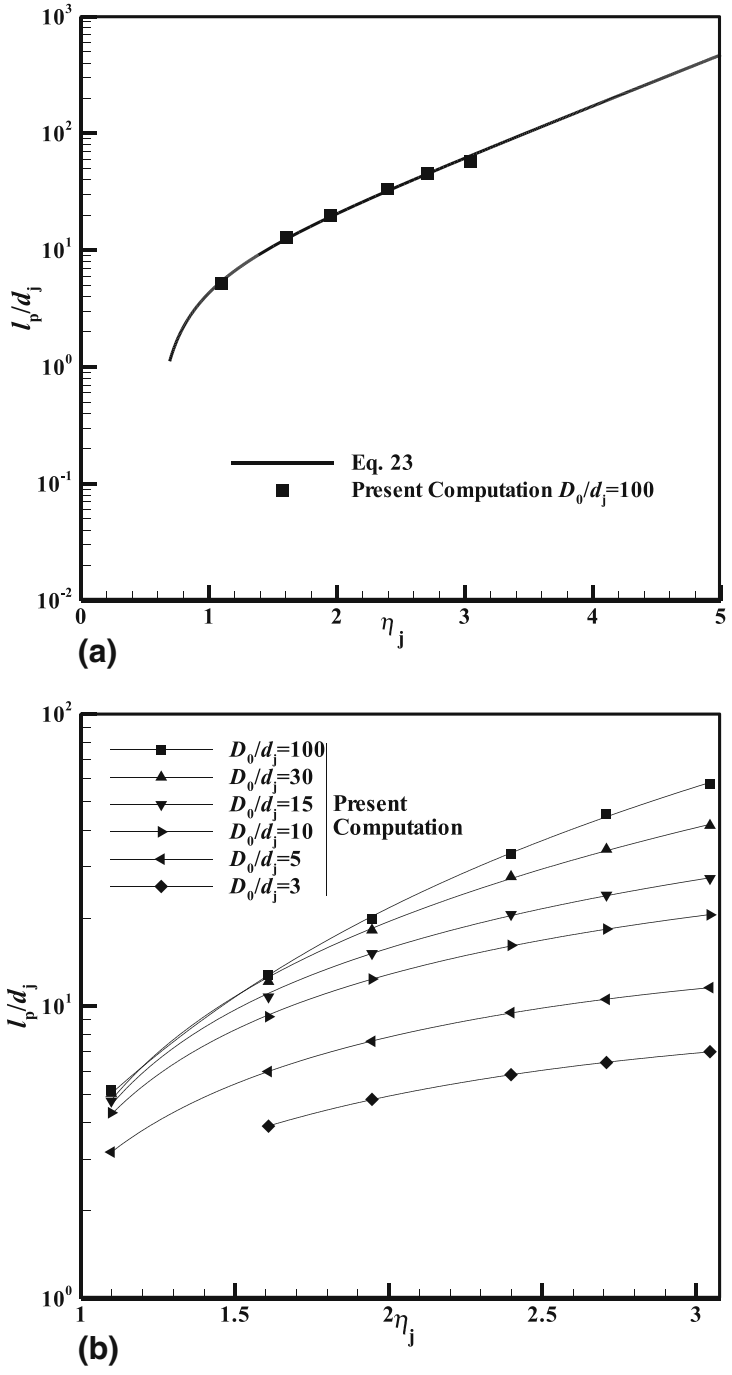

Figure 10. Non-dimensional jet penetration length, l_p/d_j, as a function of η_j from modified Oron & Abuaf (1977) similarity solution. **(a)** Comparison of present results for the highest diameter ratio considered in this study $D_0/d_j = 100$ with the modified Oron & Abuaf (1977) solution. **(b)** Present computational results for all diameter ratios.

The jet penetration length given by Eq. (23) is plotted in figure 10a along with the computational data for $D_0/d_j = 100$. There is a good agreement except at the last point with the largest value of η_j or l_p. This point violates the condition $D_0/l_p \geq 2$ (see figure 4a) and hence the penetration length is seen to be shorter. An extension of this data set for larger η_j is bound to bring about a larger deviation. This feature should be more pronounced for smaller values of D_0/d_j as can be seen in figure 10b.

The modified model with the similarity solution provides a framework for plotting the jet penetration length as a function of velocity ratio even in the presence of confinement as shown in figure 10b. Though such a plot was originally conceived for unconfined counterflow, it has been extended now to represent data for all values of D_0/d_j including those violating the condition $D_0/l_p \geq 2$.

6. Effect of jet turbulence intensity

The jet exit turbulence intensity was systematically varied to see its effect on the penetration length. The computational results reported hitherto were for a jet exit turbulence level of 4.5%. In a numerical experiment this value was reduced to 2.25% and subsequently it was increased to 9%; the results are shown in figure 11. It is observed that a higher turbulence level has decreased the length of the potential core and the jet penetration length to a lesser extent.

Such a qualitative trend may also be seen in the similarity solution by changing the value of λ. A smaller value of λ leads to lower turbulence viscosity corresponding to lower value of turbulence intensity, *Tu*, and turbulence kinetic energy, *k*. This indeed will give a slightly longer

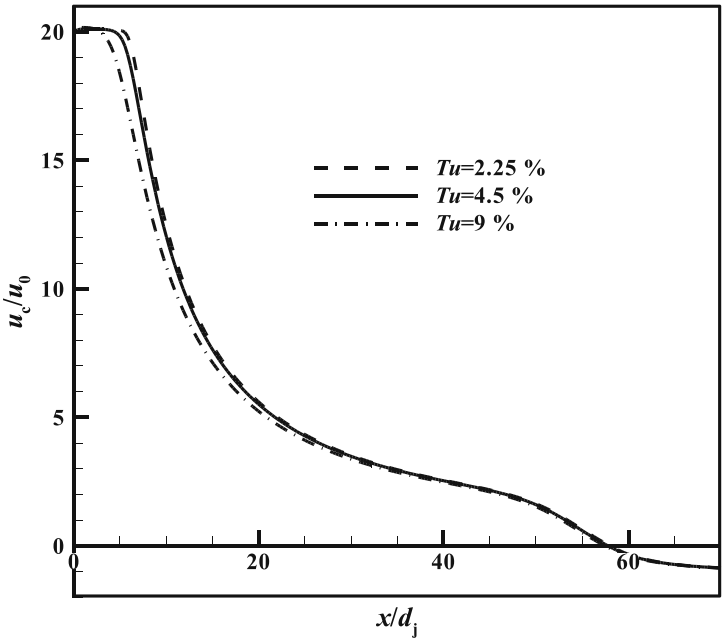

Figure 11. Effect of jet exit turbulence intensity on jet penetration length; $D_0/d_j = 100$, $u_j/u_0 = 20$. An increase in the jet exit turbulence intensity caused a reduction in the potential core and penetration lengths.

penetration length. However, its effect on the potential core as shown in figure 11 cannot be deduced from the similarity solution.

7. Conclusion

The flowfield of an axisymmetric, turbulent jet issuing into a uniform, confined counterflow was investigated computationally. The jet penetration length was found to be in good agreement with the available experimental data.

The observations of Morgan *et al* (1976) regarding dependence of jet penetration length on momentum flux ratio were derived in the present study from dimensional analysis. It was further argued that at high momentum flux ratio their observation of a distinct flow regime with the penetration length following a one-third power law is not correct. Instead of a one-third power, the power is seen to diminish continuously to zero. This led to an interesting observation that there is a limiting value of jet penetration length equal to about 3.57 times the duct diameter unlike in an unconfined case where it grows linearly with jet-to-counterflow velocity ratio. A scatter in data was observed for intermediate values of momentum flux ratio due to the presence of the potential core.

The similarity solution for the jet in unconfined counterflow proposed by Oron & Abuaf (1977) provided a good framework for comparison of both confined and unconfined cases. A modified model based on this similarity solution with the potential core being added to the penetration length led to good agreement with the computational results. Apart from giving an insight to the flowfield, this method should be of use in estimating the jet penetration length for any set of parameters.

References

Arendt J, Babcock H A and Schuster J 1956 Penetration of a jet into a counterflow. *J. Hydr. Div.* 82: 1038–8

Beltaos S and Rajaratnam N 1973 Circular turbulent jet in an opposing infinite stream. *Proceedings of 1st Canadian Hydrotechnical Conference*, Edmonton

Bernero S 2000 A turbulent jet in counterflow. Ph D thesis. Berlin: Technical University of Berlin

Brinkworth B J 1999 Discussion to Lam K M, Chan H C 1997 Round jet in ambient counterflowing stream *J. Hyd. Eng.* 123:895–903; *J. Hyd. Eng.* 125: 430–431

Chan C H C and Lam K M 1998 Centreline velocity decay of a circular jet in a counterflowing stream. *Phys. Fluids* 10(3): 637–644

Celik I B, Ghia U, Roache P J, Freitas C J, Coleman H and Raad P E 2008 Procedure for estimation and reporting of uncertainty due to discretization in CFD applications. *J. Fluids Eng.* 130: 078001-1-4

Lam K M and Chan H C 1997 Round jet in ambient counterflowing stream. *J. Hyd. Eng.* 123(10): 895–903

Morgan W D, Brinkworth B J and Evans G V 1976 Upstream penetration of an enclosed counterflowing jet. *Ind. Eng. Chem. Fundam.* 15(2): 125–127

Oron A and Abuaf N 1977 Jet expanding into a uniform counterflow. *Isr. J. Tech.* 15: 239–245

Pope S B 2000 *Turbulent flows*. New Delhi: Cambridge University Press

Saghravani S F and Ramamurthy A S 2010 Penetration length of confined counter flowing free jets. *J. Hydr. Eng.* 136: 179–182

Schlichting H 1979 *Boundary-layer theory*. New York: McGraw-Hill

Sekundov A N 1969 The propagation of a turbulent jet in an opposing stream. *Turbulent jets of air, plasma and real gas,* G N Abramovich (ed.) New York: Consultants Bureau

Yoda M and Fiedler H E 1996 The round jet in a uniform counterflow: Flow visualization and mean concentration measurements. *Exp. Fluids* 21: 427–436